**PAPER** • **OPEN ACCESS**

# Odorant binding proteins from *Hermetia illucens*: potential sensing elements for detecting volatile aldehydes involved in early stages of organic decomposition

To cite this article: Marisa Nardiello *et al* 2022 *Nanotechnology* **33** 205501

OPEN ACCESS
IOP Publishing
Nanotechnology

Nanotechnology **33** (2022) 205501 (15pp)
https://doi.org/10.1088/1361-6528/ac51ab

# Odorant binding proteins from *Hermetia illucens*: potential sensing elements for detecting volatile aldehydes involved in early stages of organic decomposition

**Marisa Nardiello[1,2], Carmen Scieuzo[2,3,5], Rosanna Salvia[2,3,5], Donatella Farina[2,3], Antonio Franco[2,3], Jonathan A Cammack[4], Jeffrey K Tomberlin[4], Patrizia Falabella[2,3,6,*] and Krishna C Persaud[1,6,*]**

[1] Department of Chemical Engineering, The University of Manchester, Manchester, United Kingdom
[2] Department of Sciences, University of Basilicata, Via dell'Ateneo Lucano 10, 85100, Potenza, Italy
[3] Spinoff XFlies s.r.l., University of Basilicata, Via dell'Ateneo Lucano 10, 85100, Potenza, Italy
[4] Department of Entomology, Texas A&M University, College Station, TX, United States of America

E-mail: krishna.persaud@manchester.ac.uk and patrizia.falabella@unibas.it

Received 17 September 2021, revised 31 January 2022
Accepted for publication 3 February 2022
Published 21 February 2022

**Abstract**

Organic decomposition processes, involving the breakdown of complex molecules such as carbohydrates, proteins and fats, release small chemicals known as volatile organic compounds (VOCs), smelly even at very low concentrations, but not all readily detectable by vertebrates. Many of these compounds are instead detected by insects, mostly by saprophytic species, for which long-range orientation towards organic decomposition matter is crucial. In the present work the detection of aldehydes, as an important measure of lipid oxidation, has been possible exploiting the molecular machinery underlying odour recognition in *Hermetia illucens* (Diptera: Stratiomyidae). This voracious scavenger insect is of interest due to its outstanding capacity in bioconversion of organic waste, colonizing very diverse environments due to the ability of sensing a wide range of chemical compounds that influence the choice of substrates for ovideposition. A variety of soluble odorant binding proteins (OBPs) that may function as carriers of hydrophobic molecules from the air-water interface in the antenna of the insect to the receptors were identified, characterised and expressed. An OBP-based nanobiosensor prototype was realized using selected OBPs as sensing layers for the development of an array of quartz crystal microbalances (QCMs) for vapour phase detection of selected compounds at room temperature. QCMs coated with four recombinant *H. illucens* OBPs (HillOBPs) were exposed to a wide range of VOCs indicative of organic decomposition, showing a high sensitivity for the detection of three chemical compounds belonging to the class of aldehydes and one short-chain fatty acid. The possibility of using biomolecules capable of binding small ligands as reversible gas sensors has been confirmed, greatly expanding the state-of the-art in gas sensing technology.

[5] CS and RS have an equal contribution.
[6] PF and KCP have an equal contribution.
[*] Authors to whom any correspondence should be addressed.



 

Supplementary material for this article is available online

Keywords: odorant binding proteins, quartz crystal microbalances, volatile organic compounds

(Some figures may appear in colour only in the online journal)

## 1. Introduction

The characteristic odour of animal and vegetable decomposition is made up of complex mixtures of volatile organic compounds (VOCs). These are low molecular weight compounds belonging to different chemical classes such as carboxylic acids, alkanes, ketones, alcohols, aldehydes, amines, sulphurous compounds and others, some of which may be perceived as pleasant smells and others highly repulsive to the human nose [1]. The olfactory thresholds for detection of some of these molecules are often at ppb levels [2], where conventional analytical instruments function poorly. Hence, the conventional method of malodour measurement is typically by dynamic dilution olfactometry using human panels [3]. High-resolution gas chromatography coupled with different mass spectrometers, secondary electrospray ionization mass spectrometry (SESI-MS), ion mobility spectrometry (IMS), selected ion flow tube mass spectrometry (SIFT-MS) and proton transfer reaction mass spectrometry (PTR-MS) have all been used but are greatly affected by sampling techniques and have limited applications [4–6].

There is widespread interest in development of sensing systems for malodours in a large number of contexts as often these indicate the presence of harmful components and can cause negative health and environmental effects [7]. Real-time monitoring of VOC concentration levels can provide useful information about the early stages of decomposition and thereby lead to the improvement of safety standards in the agri-food sector [8, 9]. Furthermore, malodorous VOCs with toxic properties from industrial production [10], sewage treatment plants [11, 12], municipal landfill sites [13], livestock and poultry production [14] and waste treatment processes [15] would benefit from early warning systems of malodour emission, because of the increasing number of complaints from the human population who live near emission sources (reviewed by Conti *et al* [3]).

### 1.1. Malodour detection systems

Because conventional analytical instruments could not be readily used for malodour monitoring in the field, many researchers have resorted to using 'electronic nose' techniques (recently reviewed by Covington *et al* [16]). Key publications include that of Schiffman and Osuna who reported the use of such a system for evaluating the odours from swine operations [1], Stuetz *et al* for sewage odour monitoring [17], Tanaka *et al* for measurement of oral malodour [18], Wilson [19] for hazardous gases, Schnürer *et al* [20] for detection of fungal volatiles indicative of food spoilage, together with networks of sensing devices for malodour monitoring [21].

Despite many research publications, all of these approaches suffered from lack of sensitivity and selectivity required for the application due to the types of gas sensors utilised (usually metal oxide gas sensors or electrochemical gas sensors). Hence, researchers have turned to utilising and adapting components of the biological olfactory system as nanolayers to create hybrid biomimetic sensing systems, where the recognition element of a gas or odour sensor is an odorant binding protein or a receptor coupled to a transducer (reviewed by Persaud [22]). These have promise in improving conventional 'electronic nose' systems to the level where they can be utilised for routine odour detection and measurements. The frontier of nanotechnology is heading towards the development of increasingly miniaturized devices and the use of biological components as nanolayers opens new possibilities in this field.

*1.1.1. Odorant binding proteins.* The chemosensory organs of vertebrates and insects contain a family of proteins that are associated with detection and release of chemical stimuli [23, 24]. They are present in very high concentrations, have rapid turnover, and are involved in the binding of numerous hydrophobic ligands with dissociation constants typically in the micromolar range. Several types of OBPs may be expressed in the same species. Divergence in their amino acid sequences indicates that these proteins can selectively bind different classes of odorants. OBPs of vertebrates belong to the family of lipocalin proteins reviewed by Flower [25, 26] while those of insects are folded into $\alpha$-helical domains [27, 28]. Much information is now available on OBPs and related proteins from many vertebrate and invertebrate species and the role they play in supporting the chemical sensing is now becoming clearer. They are extremely stable to temperature, organic solvents and proteolytic digestion. Their nanoscale dimensions (1–2.5 nm) are attractive for immobilization onto the surface of a transducer, to convert the analyte binding into a recordable signal, which is a great asset for fabricating biosensors. For biotechnological applications, OBPs can be expressed in bacterial systems at low cost and are easily purified [29]. The large amount of information available on their structures and affinities to different molecules also allows the design of specific mutants that can be tailored to bind chemical species of interest. Some similar proteins such as pheromone-binding proteins (PBPs) [30], major urinary proteins (MUPs) in rodents [31, 32] or salivary lipocalin (SAL) in the boar [33, 34] are clearly involved in vertebrate chemical communication, binding with high specificity sex pheromone components. Pelosi and co-workers extensively reviewed the scope of applying OBPs in biotechnological applications [35], highlighting the possibilities of site directed mutations of various OBPs to change the target ligands to those desired by a target application. Ricatti *et al* [36] documented the effects of point mutations in the binding pocket of the closely related protein family mouse major urinary protein (MUP20) and the repercussions on ligand affinity and specificity.

Persaud and Tuccori [37, 38] showed that an array of biosensors could be easily constructed based on immobilization of odorant binding proteins onto suitable transducers. An

important consideration for the biosensors development is the immobilization of the bio-recognition element following self-assembly processes that maximize overall activity and minimize structural changes. As the first step in the immobilization process, the self-assembled monolayer offered advantages to the proteins used at nanoscale levels such as the chemical stability and the spontaneous orientation of the binding pockets at the air-support interface. Using a quartz crystal microbalance platform as a transduction element, it was possible to detect and measure quantitatively concentrations of volatile analytes at parts per million concentrations in air. A number of publications have demonstrated that immobilisation of OBPs on acoustic wave or mass balance transducers produce stable sensors that can be utilised in a wide variety of applications [39–42].

### 1.2. Hermetia illucens

*Hermetia illucens* (Linnaeus, 1758) (Diptera: Stratiomyidae) is a bioconverter insect commonly known as the Black Soldier Fly (BSF). It is one of the most studied insect species for the bioconversion of organic waste and it is a promising and sustainable source of proteins, lipids, and bioactive compounds (i.e. chitin and antimicrobial peptides) [43–48]. Adult gravid females are attracted by VOCs coming from decomposing organic substrates and some species of bacteria normally present on decaying matter [49]. Once laid nearby organic matter, eggs hatch after 3 days and the newborn larvae, also thanks to their strong mouthparts and specific digestive enzymes, voraciously feed for 15–20 days on a variety of decomposing substrates of both plant and animal origin, including fruits, vegetables, human and animal faeces, manure and carrion, previously selected by the ovipositing females [50–55]. The work presented here develops previous research by Scieuzo *et al* [56] who investigated the larval and adult transcriptome and reported an in-depth study of potential OBPs involved in odour recognition in *H. illucens*. This organism has evolved an arsenal of OBPs, with different grades of gene expression, that allow the colonization of the most disparate environments with characteristic smells of decomposition. These OBPs may have specific functions in the behaviour of the insect and the choice of appropriate substrates for deposition of eggs.

The opportunity to incorporate these natural proteins, able to bind volatile products of decomposition, for the development of innovative biosensors mimicking the biological system has been exploited in the present work. Available data on the three-dimensional structures and diameter of the main binding pockets [56] confirmed their use for the development of biosensors at nanoscale, offering significant advantages in terms of enhanced detection sensitivity and specificity. Here, we report the expression, characterization and performance of immobilised *H. illucens* OBPs (*Hill*OBPs) on quartz crystal microbalance transducers, capable of sensitively detecting chemical species associated with organic decomposition.

## 2. Materials and methods

### 2.1. Reagents, bacterial strains and plasmids

Analytical grade reagents for RNA purification, bacterial growth and chemicals were of analytical grade purchased from Sigma-Aldrich, Fisher Scientific or VWR (UK). T4 DNA Ligase and *Eco*RI/*Bam*HI restriction enzymes were supplied by New England Biolabs (USA). Primers were synthesized by Macrogen Europe (Netherlands), SuperScript® for RT-PCR was ordered at Invitrogen (USA) and the KOD DNA Polymerase at Merck Millipore (USA). DH5-α and BL21 (DE3) *Escherichia coli* chemically competent cells were purchased respectively from Invitrogen (USA) and Agilent (UK). For the molecular cloning pCR™II-TOPO® vector was ordered at Thermo Fisher, while pET-22b(+) vector was kindly provided by Prof. Paolo Pelosi (Italy). Plasmid mini/midi kit, Gel extraction kit and HiPrep™ and HisPrep™ columns were obtained respectively from Invitrogen (USA), Bio-Rad (USA) and GE Healthcare (UK), dialysis membrane tubing was ordered at the Spectra/Por® (USA). The JLMQ USB interface for 4 QCM sensors (JLM Innovation GmbH, Tuebingen, Germany) was used as a readout system for 20 MHz quartz crystal microbalances with gold coated electrodes fabricated by IMM-CNR (Italy). Odorants, purchased from Sigma-Aldrich (UK), were diluted in recommended solvents (https://pubchem.ncbi.nlm.nih.gov/) for *in vitro* binding assays by using a quartz cuvette with a light path of 1 cm (Quartz Suprasil 10 mm, Hellma) and freshly used without any dilutions on the day of the experiments in glass vials (Supelco, 40 ml) for biosensor acquisition. The fluorescent probe used to measure the binding activity in solution was the N-phenyl-1-naphthylamine (1-NPN), provided by Sigma-Aldrich (UK).

### 2.2. RNA extraction, RT-PCR and cloning of HillOBP genes

RNA was isolated from 500 mg of *Hermetia illucens* larvae using TRI-Reagent, following the manufacturer's protocol and the purified RNA sample was stored at −80 °C until use. In order to remove all the genomic DNA contaminations, total RNA (5 $\mu$g) was treated with DNAse I and the full-length cDNA synthesis was performed in a reaction mixture containing dNTP mix (10 mM), oligo $(dT)_{20}$ primers (50 $\mu$M) and the SuperScript III RT (200 U $\mu l^{-1}$). The full length of *H. illucens* OBP (*Hill*OBP) genes was synthesized following conditions established for the reverse transcriptase and amplified by conventional polymerase chain reaction (PCR) (Thermocycler, Applied Biosystems) using specific primers (table S1). Primers related to specific contigs were named wild-type (WT) and six histidine tagged (HisTag) (WT-OBP_C57; HisTag-OBP_C11107; HisTag-OBP_C21691; HisTag-OBP_C1173); the *Eco*RI and *Bam*HI sites were added to the forward and reverse primers, respectively. Amplicons were generated starting from 1 $\mu$l of cDNA template in a 50 $\mu$l of solution containing saline buffer (10X), dNTP mixture (2 mM), $MgCl_2$ (25 mM), forward and reverse primers (10 $\mu$M each), KOD® High Fidelity DNA polymerase

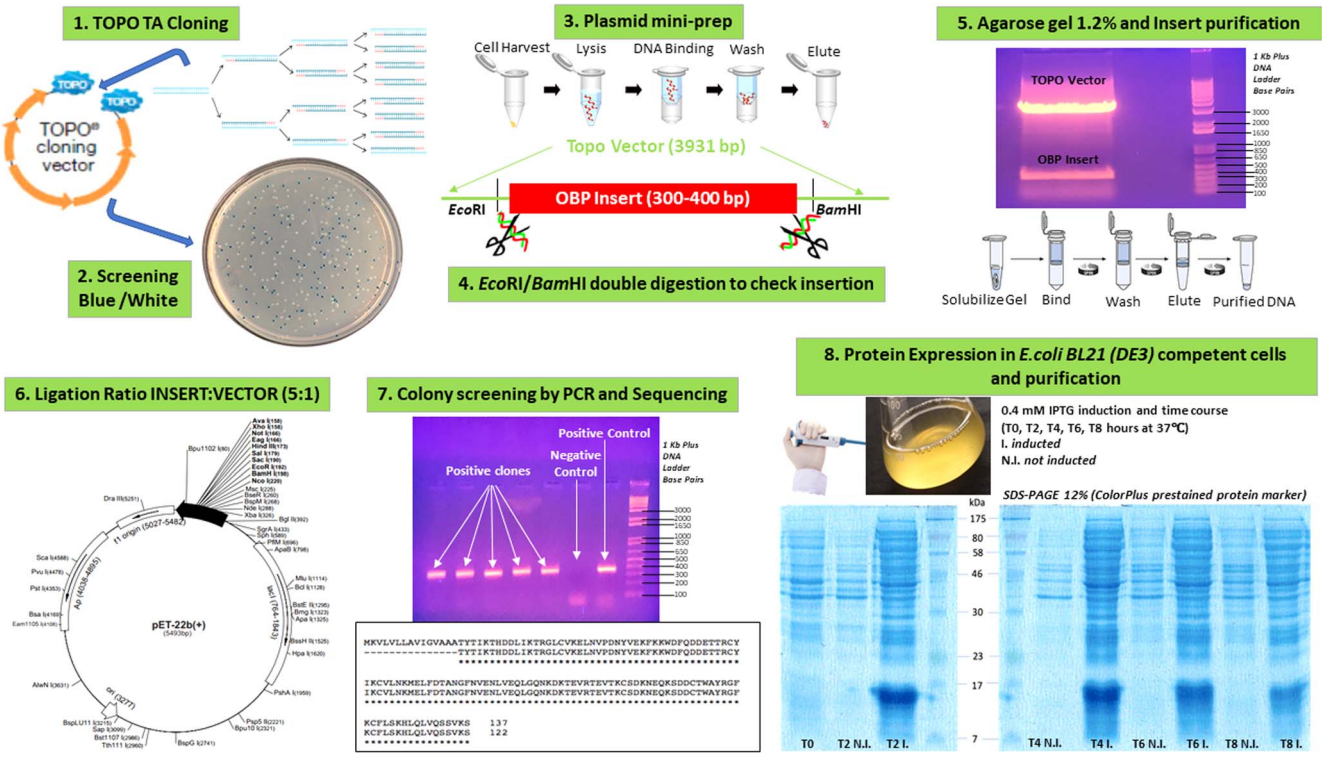


**Figure 1.** Production of *Hermetia illucens* Odorant Binding Proteins (*Hill*OBPs) using recombinant DNA technology. After subcloning *Hill*OBP genes in pCR™II-TOPO® vector (1), positive clones from white colonies screening (2) were subjected to a *Eco*RI/*Bam*HI restriction digestion (4, 5) and ligated with T4 DNA ligase into the expression vector pET-22b(+) (6). Positive colonies (7) was subjected to an eight-hour time course which was used to monitor the *Hill*OBPs production and the protein pattern was checked by SDS-PAGE gel (12.5%), under reducing conditions and Coomassie Blue R-250 staining (8) (N.I., not induced, I. induced).

(2.5 U $\mu l^{-1}$). PCR conditions were used according to the polymerase protocol and each amplicon was electrophoresed on 1.2% (w/v) agarose gel, stained with UltraPure™ Ethidium Bromide (0.5 $\mu$g $ml^{-1}$) (Thermo Fisher). The PCR product was first cloned in pCR™II-TOPO® following the manufacturer's protocol. Then DNA from positive colonies was digested with *Eco*RI and *Bam*HI and then ligated with T4 DNA ligase into the *Eco*RI/*Bam*HI-treated pET-22b(+) vector (30 ng), following the manufacturer's protocol. The entire volume of ligation reaction was used to transform *E. coli* DH5-α cells with heat shock method (30 min in ice—45 s at 42 °C–5 min in ice) and clones were propagated growing in a Luria–Bertani (LB) broth at 37 °C. The clone selection was carried out in plates with LB agar to which was added 50 $\mu$g $ml^{-1}$ ampicillin ($Amp^R$). Screening of *E. coli* clones was carried out using the Colony-PCR technique and the final recombinant plasmids were isolated using the FastPlasmid™ Mini kit (5 PRIME). DNA fragments were sequenced and analysed with Clustal Omega (https://www.ebi.ac.uk/Tools/msa/clustalo/) setting the parameters by default, in order to verify the sequence fidelity.

### 2.3. Expression and purification of recombinant HillOBPs

The steps involved in the production of OBPs are outlined in figure 1.

The heterologous expression of recombinant *Hill*OBPs was carried out with specific plasmids transformed in *E. coli* BL21 (DE3) pLys and inoculated in 1 l of LB medium supplemented with 50 $\mu$g $ml^{-1}$ ampicillin ($Amp^R$). Isopropyl-ß-D-thiogalactoside (IPTG) (0.4 mM) was added when the optical density ($O.D._{600\ nm}$) value reached 0.6 at 37 °C, shaking at 225 rpm for 2 h. After expression, cells were harvested by centrifugation at 4000 rpm (4 °C) for 20 min and resuspended in equilibration buffer (50 mM Tris-HCl, pH 7.4), with addition of phenylmethylsulfonyl fluoride (PMSF) (1 mM). The cell suspension was passed through a sonicator (Bandelin Sonopuls) to give a crude cell-free supernatant enriched with soluble proteins, which was clarified by centrifugation at 4000 rpm (4 °C) for 2 h. The *Hill*OBPs extraction was optimized treating the pellet with lysis buffer (50 mM Tris-HCl, 0.5 M NaCl, 8.0 M Urea, pH 7.4) added with dithiothreitol (DTT) (1 mM), and stirring for 1 h at room temperature, in order to release insoluble proteins from the inclusion bodies. A centrifugation at 4000 rpm (4 °C) for 20 min to remove insoluble cellular debris was followed by four cycles of dialysis at 4 °C for 16 h in Spectra/Por® dialysis membrane tubing (MWCO, 12–14 kDa) against equilibration buffer to dilute salts and favour the protein refolding. Ion exchange (IEX) and affinity chromatography were, respectively, the two techniques performed for the purification of the wild-type *Hill*OBP_C57 and 6-His-tagged *Hill*OBPs (C-ter: *Hill*OBP_C11107, *Hill*OBP_C21691; N-ter:

*Hill*OBP_C1173), according to the manufacturer's instructions. For the purification of *Hill*OBP_C57, the crude extract was loaded to a HiPrep™ Q Sepharose Fast Flow 16/10 column, pre-equilibrated with equilibration buffer (50 mM Tris-HCl, pH 7.4) and the bound *Hill*OBP_C57 was eluted with elution buffer (50 mM Tris-HCl, 0.5 M NaCl, pH 7.4). The HisPrep™ Fast Flow 16/10 column, pre-equilibrated with equilibration buffer (50 mM Tris-HCl, 500 mM NaCl, 35 mM Imidazole, pH 7.4) was used to purify the remaining 6His-tagged *Hill*OBPs. The crude extracts, to which imidazole (35 mM) was previously added, were loaded into the column and, thereafter, the bound *Hill*OBPs were separately eluted with the same buffer, with addition of imidazole (500 mM). The eluates were analysed in 12.5% (w/v) SDS-PAGE gels and stained with 0.1% (w/v) Coomassie brilliant blue (R-250) to confirm the presence of *Hill*OBPs free of contaminants. The molecular weights, predicted with ProtParam —ExPASy tool, were confirmed using Novex™ Sharp pre-stained protein marker and the concentration was estimated using bovine serum albumin (BSA) as a standard [57], and the Beer–Lambert's law [58].

### 2.4. Delipidation and ultrafiltration of purified recombinant HillOBPs

A delipidation treatment was used to decrease non-specific binding from any pockets of the recombinant *Hill*OBPs produced in *E. coli* cells, as trapped endogenous lipids could affect the active sites of proteins. The fatty acid residues were easily removed, without denaturing or permanent loss of *Hill*OBPs binding activity, by using 1.0 g of pre-swollen Sephadex LH-20 in 50 mM sodium acetate buffer pH 4.5, was shaken for 3 h at room temperature. The slurry was spin washed twice with the same buffer and then equilibrated with 25% (v/w) of the same buffer. The protein samples pH was adjusted to 4.5 with acetic acid, mixed with the slurry (5:1) and stirred at 4 °C for 1 h. The supernatant, cleaned from fatty acids previously trapped in the slurry, was collected following two centrifugation steps at 15 000 g (4 °C) for 5 min. Finally, the supernatant containing protein was dialysed overnight against 50 mM Tris-HCl pH 7.4, centrifuged and filtered with a 0.8 $\mu$m filter. The diluted protein fractions were transferred to Amicon® Ultra-15 Centrifugal Filter Devices with a 10 kDa molecular weight cut-off regenerated cellulose membrane (Merck Millipore) and centrifuged at 4000 rpm (4 °C), for a protocol time adapted to obtain a volume equal to 1/10 compared to the initial volume and, as consequence, higher concentration values per milliliter.

### 2.5. Fabrication of QCM-based biosensors

The AT-cut quartz crystal was sandwiched between two gold electrodes, with a diameter of 7.95 mm for the crystal and 4.9 mm for the geometric surface of the gold layer, to build a quartz crystal microbalance (QCM) (figure 2). The golden electrodes were sputtered on the quartz crystal on an adhesion layer of titanium. The QCM was driven by a Pierce oscillator circuit that created a oscillating electric field of 2.4 V amplitude which induced an acoustic wave. The thickness of QCM determined a base resonant frequency of approximately 20 MHz. In the AT-cut crystal, the temperature dependence of the resonant frequency is known to be negligible in the range of 0 °C–40 °C. The QCM gold surface was cleaned by dipping the crystal into a strong oxidizer Piranha solution (1:3, 30% $H_2O_2$: $H_2SO_4$) for 4 min, to remove any organic contaminants from the gold surface and allow the deposition of the self-assembled monolayer. QCMs were then thoroughly rinsed with distilled water, absolute ethanol and dried at air, before starting the protein immobilisation process.

### 2.6. Immobilization of HillOBPs on the QCM surface

Prior to the deposition of *Hill*OBPs, the gold electrode surfaces were chemically modified with thioctic acid (TA), an alkanethiol used as self-assembled monolayer (SAM). The assembly of the lipid layer was favoured by immersion of QCMs into a solution of 10 mM TA in ethanol for 20 h under nitrogen flow (20%), to allow a higher efficiency of TA binding on the gold surface. To remove any unbound molecules of TA, the electrodes were then rinsed twice with absolute ethanol and left to dry at room temperature. TA free carboxylic groups were activated through a reactive intermediate, pipetting alternately on the both sides of gold surface 20 $\mu$l of a solution, composed of 180 mM ethyl-(dimethylaminopropyl)-carbodiimide (EDC) and 180 mM of N-hydroxy-succinimide (NHS) in 10 mM sodium phosphate buffer (pH 7.0). The SAM activation process lasted for 2 h at room temperature and was then interrupted with two washes in distilled water. QCMs were dried in air, 10 $\mu$l of protein solution (0.3–1.5 mg $ml^{-1}$) was pipetted over the gold surface of each electrode and left for 1 h at room temperature, to create the peptide bonds between the amino groups in R side chains of *Hill*OBPs and the activated carboxylic groups of SAM. Each deposition process was followed by rinsing with distilled water and drying at air, three times for each QCM side. The QCM gold area was coated with the peptide monolayer, fixed to the SAM by a covalent bond; the thick film of the unbound fluid was removed manually after the deposition, avoiding contact with the outer edge of each crystal.

### 2.7. Biosensor test with vapour of the target analytes

The acquisitions were carried out under strictly controlled conditions in terms of resonance frequency of the microbalances, in order to obtain a stable baseline. The surface coverage of QCM resonator with *Hill*OBPs as sensing layer and the adsorption of analyte molecules to characterize the binding interactions with this biochemical recognition film were monitored by variations in the resonance frequency expressed by the Sauerbrey equation [59], where, $\rho_q$ and $\mu_q$ are the density (2.648 g $cm^{-3}$) and shear modulus ($2.947 \times 10^{11}$ g $cm^{-1}$ $s^2$) of the quartz, $f_0$ is the fundamental frequency of the piezoelectric quartz crystal (19453 $\pm$ 50 KHz) and $A$ is the crystal piezoelectrically active geometrical surface (0.496 $cm^2$), that is the area of the deposited film on

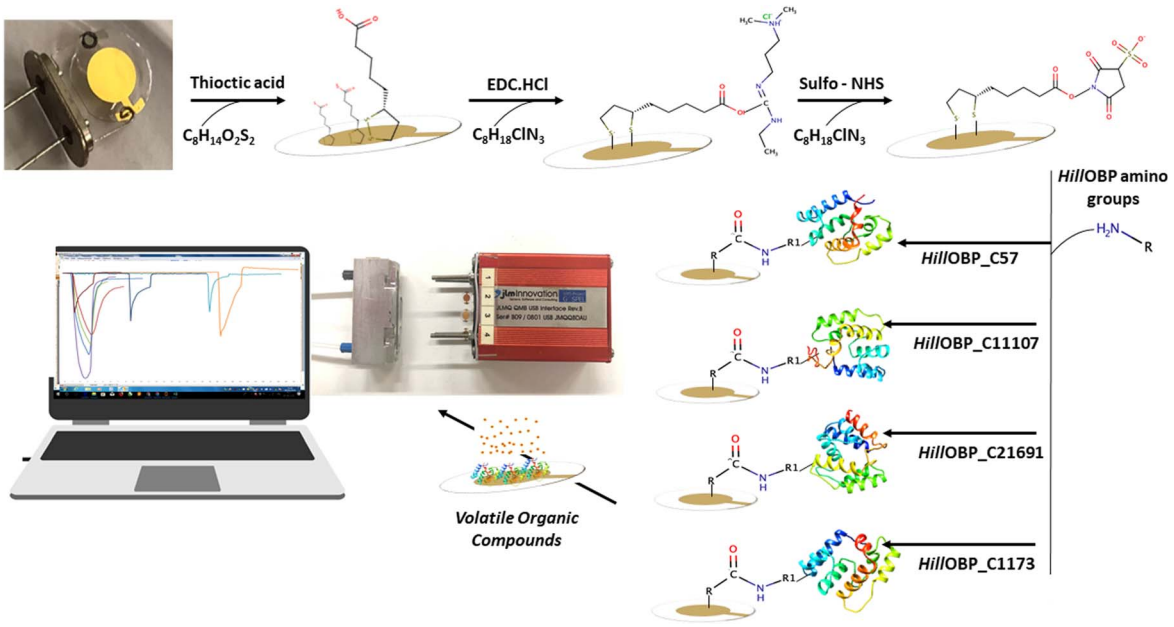


**Figure 2.** Immobilization process of recombinant *Hill*OBPs by using thioctic acid (TA) as self-assembled monolayer (SAM). The TA disulphide atoms strongly bound the gold QCM surfaces with a covalent bond and the carboxylic acid groups were then activated by using an EDC/NHS solution. *Hill*OBPs were tightly attached on QCMs with peptide bonds occurring between the free amino groups of R chains and the activated carboxylic acid groups of TA.

the gold electrode. According to this equation, there is a decrease in the system frequency proportional to the mass changes ($\Delta m$), as a consequence of the material deposition on the crystal surface. The frequency shift ($\Delta f$) was used to calculate the number of *Hill*OBP molecules immobilised on each QCM and monitor the VOC interactions. To provide evidence that the response signals obtained from the biosensor are specific, a series of control measurements have been included. Firstly, QCM devices fabricated and functionalized with the SAM, but without immobilised *Hill*OBPs, were tested. The response of the biosensor was also tested with 2-phenylethanol, a compound recognized as a ligand with poor binding affinity to insect OBPs, on the basis of experiments performed in Cali and Persaud [42]. The resulting *Hill*OBP-based sensors were then exposed for 20 s to pulses of vapours from target VOCs indicative of organic decomposition. QCM measurements with JLMQ USB interface with *MultiSens* software (JLM Innovations, Germany) were performed at room temperature with a relative humidity (RH) of 22% and, between each acquisition, the baseline was established with clean air flowing at the rate of 20 ml $min^{-1}$.

### 2.8. In vitro fluorescent competitive binding assays

Fluorescent competitive binding assays were employed for a functional characterization of *Hill*OBP_C57, previously identified as the OBP expressed at the highest level in *H. illucens* [56] and the most powerful target in the nanobiosensor assembled in the present work. All the *in vitro* interactions between *Hill*OBP_C57 and VOCs of interest were monitored using the fluorescent probe N-phenyl-1-naphthylamine (1-NPN) and measuring the fluorescence variations produced following the competition between 1-NPN and the ligand of interest for the same binding pocket. To establish the probe dissociation constant ($K_D$), 1-NPN was added in different concentrations (0–16 $\mu$M) to the Tris-HCl buffer (50 mM, pH 7.4) containing *Hill*OBP_C57 (2 $\mu$M) and excited at the specific wavelength of 337 nm, with an emission spectrum recorded between 380 and 450 nm. Fluorescence signals were measured with each addition of 1-NPN and, as result, the intensity increased several fold with a shift of the emission wavelength to a maximum of 407 nm. The $K_D$ of ligands was measured using Tris-HCl buffer (50 mM, pH 7.4) containing *Hill*OBP_C57 (2 $\mu$M) and 1-NPN (5 $\mu$M), titrated with solutions of each ligand to final concentrations of 0–16 $\mu$M. The fluorescence measurements were performed in three replicates on a Perkin Elmer LS-55 Luminescence Spectrometer at 25 °C in a right-angle configuration, with 5 nm of slit widths on the excitation and emission monochromators. Emission fluorescence was monitored with a scan speed of 300 nm $min^{-1}$ and spectra were recorded by *FL WinLab* software. The $K_D$ for the *Hill*OBP_C57/1-NPN complex was calculated with *SigmaPlot*™ 12 (Systat Software, Inc.) (www.sigmaplot.com) and the equation $K_D = IC_{50}/1+([1\text{-NPN}]/K_{D,1\text{-NPN}})$ was used to calculate the dissociation constant of *Hill*OBP_C57 for each tested ligand, where $IC_{50}$ is the probe concentration required to occupy 50% of pockets, halving the maximum fluorescence intensity.

### 2.9. Data analysis

Nine independent replicates were obtained starting from three data acquisitions for each VOC, tested on three different QCMs, assembled in series with the same *Hill*OBP stock. Raw sensing data relating to the interactions with VOCs were normalised on the basis of the number of calculated

immobilised *Hill*OBPs on the sensor surface. The related frequency curves and the different VOC concentrations allowed to study the kinetics of adsorption and desorption, in order to extrapolate useful information related to dissociation constants, affinity, sensitivity and limit of detection (LOD) of the *Hill*OBP-VOC complex. Inspection of multidimensional data sets from an array of different OBPs responding to individual VOCs was performed using Principal Component Analysis (PCA) [60–62]. PCA is a general mathematical method of extracting significant information from a large complex data set, by projecting data in a global model in this case of protein-ligand space. As an orthogonal regression in the space, PCA defines the structure of variance–covariance of a data set through a system of coordinates whose number of dimensions is less than the number of original variables.

A neural network based on radial basis functions (RBF) was used to test discrimination between malodour types. A confusion matrix shows the overlap and discrimination power of datasets measuring the separability of classes and predict the binding propensities of each VOC towards a given *Hill*OBP. Values were in the range of 0 and 1, values lower than 0.5 showed a rather bad separability, while high values, near 1, indicated a good separability of classes.

## 3. Results

### 3.1. Hermetia illucens Odorant Binding Proteins (HillOBPs) as sensing nanolayers

Based on the *de novo* transcriptome analysis [56], four different *Hill*OBPs (*Hill*OBP_C57, *Hill*OBP_C11107, *Hill*OBP_C21691 and *Hill*OBP_C1173) were expressed as recombinant proteins in a heterologous system. To determine the influence of 6His-tag on the protein structure, *Hill*OBP_C57 was cloned without tag, *Hill*OBP_C11107 and *Hill*OBP_C21691 with tag at C-terminal and *Hill*OBP_C1173 at N-terminal. Each nucleotide sequence was subcloned in pCR™II-TOPO® and, after an *Eco*RI/*Bam*HI restriction digestion, it was fused to the 3′-end of the expression vector pET-22b(+) and the resulting recombinant plasmid was propagated in DH5-α and then expressed in BL21(DE3) *E. coli* competent cells (figure 1). Recombinant *Hill*OBPs were detected in purified fractions and all the observed molecular weights were compatible with the predicted size of the mature full-length recombinant proteins (table S2). In the case of 6His-tagged *Hill*OBPs, the best purification yields were obtained by coupling affinity chromatography with anion exchange chromatography, because the presence of tag was not enough to improve the purification yields, as the protein was folded into a hydrophobic conformation. Once delipidated and concentrated, *Hill*OBPs were immobilized and used as biorecognition elements on QCMs, to test the ability to detect volatile organic compounds (VOCs) of interest associated with organic decomposition.

The *Hill*OBPs immobilization, through a covalent binding between the alkanethiols of the self-assembled monolayer (SAM) and the free amino groups of the protein side chains, resulted in an easy, fast and inexpensive technique for the QCM-based biosensors technology (figure 2). A Pierce oscillator circuit allowed the quartz crystal to oscillate with its own resonance frequency (∼20 MHz), according to the phenomenon of piezoelectricity and, considering the molecular weight, the *Hill*OBP surface densities on the QCM devices were calculated. The experimental measurements of biomolecular interactions between OBPs and VOCs are based on the one-to-one binding mechanism, arised from properties of the molecules involved. On that basis, it was possible to estimate the VOCs loading per unit area ($cm^2$) (table S3).

### 3.2. Binding curves of HillOBP_C57 with the fluorescence reporter and odorants

Competitive binding assays were used to investigate *in vitro* the *Hill*OBP_C57 binding affinities, exploiting a competition between free ligands and the 1-NPN fluorescent reporter for the same main binding pockets. When excited at 337 nm in presence of *Hill*OBP_C57, 1-NPN showed a strong emission spectrum shift from 450 nm to approximately 380 nm, as well as a drastic increase in fluorescence intensity, suggesting the 1-NPN suitability for investigating in general OBP binding properties in fluorescent competitive assays. Titration with the best *Hill*OBP_C57 concentration (2 $\mu$M), chosen on the basis of background noise-free signal, and increasing concentrations of 1-NPN (0–16 $\mu$M), provided a dissociation constant ($K_D$) equal to 3.27 ± 0.54 $\mu$M (figure 3(a)). Subsequently, the fluorescence quenching by a competitive ligand was measured by adding aliquots (0–16 $\mu$M) of VOCs to the protein solution (*Hill*OBP_C57, 2 $\mu$M) pre-equilibrated with 5 $\mu$M of 1-NPN probe (figure 3(b)). All titrations showed a great reduction in fluorescence intensity and, as consequence the highest binding affinities, in presence of three specific compounds (isobutyraldehyde, isovaleraldehyde and 2-methylbutyraldehyde), belonging to the same chemical class (aldehydes) (figure 3(c)). The low values of the binding affinities recorded for the remaining compounds are not reliable since the nature of the VOCs, strongly hydrophobic, could alter the result following the micelles formation, particularly in presence of fatty acids [63, 64].

### 3.3. Interaction of recognition layer-coated quartz crystal electrode with analyte

When a QCM is loaded with a thin rigid film, which is purely elastic, the resonance frequency decreases with increased mass. If the film is much thinner than the thickness of the resonator, the decrease in resonance frequency ($f$) is linearly correlated to the increase in mass ($m$) (or thickness) according to the Sauerbrey relation:

$$\Delta m = -C\frac{\Delta f}{n}, \tag{1}$$

where $C$ is a constant dependent on the material and $n$ is the overtone number which is 1 in this case indicating the fundamental frequency. However, if a viscous component is introduced as well, such as a protein, this gives a viscoelastic

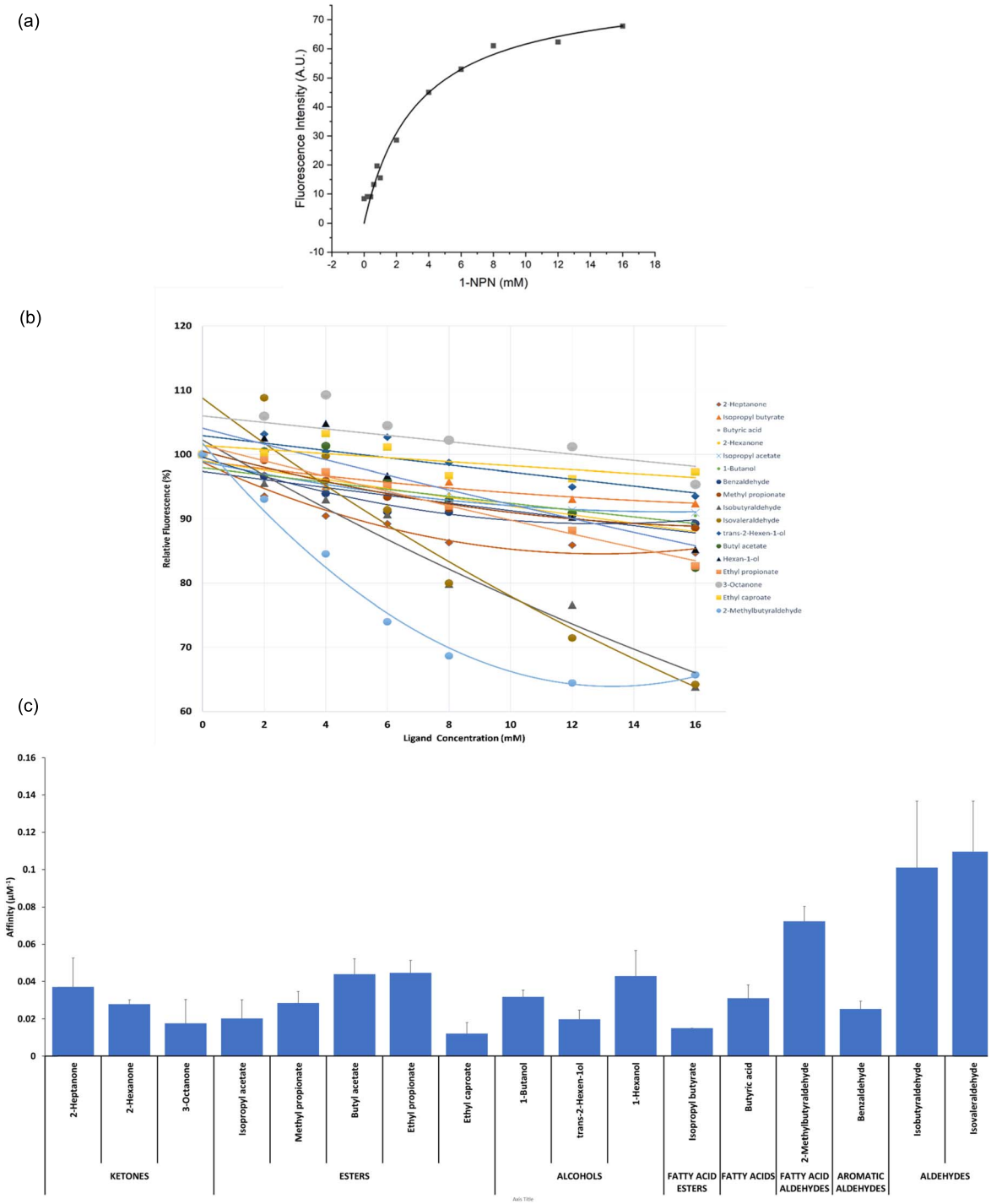


**Figure 3.** Fluorescent competitive binding assays. (a) Binding curve for N-phenyl-1-naphthylamine (1-NPN) to recombinant *Hermetia illucens* OBP_C57 (*Hill*OBP_C57). The *Hill*OBP_C57 solution (2 $\mu$M) in 50 mM Tris-HCl buffer (pH 7.4) was titrated with a solution of 1-NPN (1 mM) in methanol to final concentrations of 2–16 $\mu$M. Binding curves were measured for other *Hill*OBPs (data not shown) and the dissociation constants (mean of three replicates $\pm$ standard deviation) were: *Hill*OBP_C57: 3.27 $\pm$ 0.54 $\mu$M, *Hill*OBP_C11107: 5.48 $\pm$ 1.84 $\mu$M, *Hill*OBP_C21691: 5.27 $\pm$ 1.82 $\mu$M and *Hill*OBP_C1173: 2.49 $\pm$ 0.27 $\mu$M. (b) Competitive binding of selected ligands to *Hill*OBP_C57. A mixture of *Hill*OBP_C57 and 1-NPN in 50 mM Tris-HCl buffer (pH 7.4), at the concentration of 2 and 5 $\mu$M, respectively, was titrated with a 1 mM solution of each competing ligand to final concentrations of 2–16 $\mu$M. Fluorescence intensities were reported as percent of the values in the absence of competitors. (c) Relationship between different functional groups of tested ligands and affinity values of *Hill*OBP_C57, calculated from fluorescent competitive binding assays.

or soft film and there will be energy losses in the system, quantified by an energy dissipation factor, $D$. Depending on the conformation of the protein and how it may change in shape when it binds a ligand, the resonance frequency, $f$, and energy dissipation factor of the QCM can enter a nonlinear regime where propagation of the shear wave, and the softness of the film, will have a dampening effect on the oscillating motion quantified by $D$.

The biosensor response was investigated with 42 VOCs indicative of organic decomposition [56], by monitoring the frequency changes when the *Hill*OBP-coated QCMs were exposed to VOC vapours at a fixed concentration of 4 ppm. During the exposure phase, the *Hill*OBPs on QCMs act as recognition layers for VOC molecules and the complex formation causes a mass increase in real time that leads to a proportional reduction in the resonance frequency of the microbalances. The system showed a fast and reversible response within 20 s starting from the exposure, following the introduction of a specific analyte in vapour-phase by pumping. The baseline value was restored during the regeneration phase, when the adsorbed VOC molecules were released by switching to clean air and the frequency of the sensors rose as the mass decreased. The complete desorption of VOC vapours, achieved by injecting fresh air in the sensing chamber until the frequency returned to baseline, was indicative of good reversibility and recovery of the device. In presence of different VOCs, during a constant time of acquisition, *Hill*OBP_C57, *Hill*OBP_C11107 and *Hill*OBP_C1173 sensors had a much stronger response with a negative frequency shift only in presence of isobutyraldehyde, isovaleraldehyde, 2-methylbutyraldehyde and butyric acid. The same VOCs evoked an opposite response from the *Hill*OBP_C21691 sensor with an increase in frequency, interpretable as change in viscoelastic properties of the OBP layer. Computational analysis of this OBP indicated it was devoid of pockets involved in ligand-binding for these ligands, and the interaction with the aldehydes and fatty acid may be entirely due to surface adsorption. The frequency responses of *Hill*OBP_C57, *Hill*OBP_C11107 and *Hill*OBP_C1173 sensors decreased immediately after analyte injection and reached an equilibrium state approximately after 5–10 s, indicating a faster response time only for these specific ligands (figure 4). Data relating to VOC interactions have been normalized by multiplying the frequency variation of each analyte by the number of immobilized *Hill*OBP molecules (table S3). Sensors respond to analytes irrespective of different ambient humidity levels. Figure S1 (available online at stacks.iop.org/NANO/33/205501/mmedia) shows the QCM resonance frequencies at 22%RH, and the changes in frequencies for two immobilized proteins (HillOBP_C57, HillOBP_C11107) without VOCs (blue line, Humidity) and with analytes at 22%RH. After normalizing the data vectors across the array of QCM sensors, principal component analysis (PCA) was used to reduce the multidimensional space (i.e. responses from four independent sensors) towards the 42 VOCs, without losing information of the technical replicates. Of practical interest is not the discrimination between individual chemical species but between compounds related to spoilage origin (in this case either microbial or chemical decomposition).

The *Hill*OBP-sensor responses were presented on a PCA score plot, dividing the analysed VOCs in two main categories, related to the spoilage origin (microbial and chemical), based on the most common causes of organic degradation, such as the presence of contaminants, physical/chemical agents and animal activity (table S4). The dataset was projected onto the three-dimensional space spanned by the vectors (principal components) that correspond to the maximum variance of the dataset.

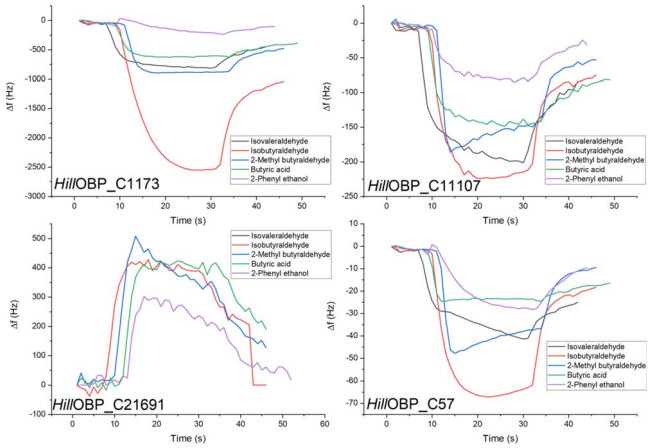


**Figure 4.** Quartz Crystal Microbalances (QCM) based responses to analyte vapours. This shows normalised changes in frequency observed for four immobilised *Hill*OBPs (table S3) when exposed to 4 ppm of Isovaleraldehyde, Isobutyraldehyde, 2-Methylbutyraldehyde, Butyric Acid and Phenyl ethanol vapour for 20 s from a baseline in clean air.

The PCA score plot indicated that the device is generally able to discriminate between microbial and chemical spoilage, however with some overlap of signals between microbial and chemical spoilage, due to the fact that all the produced VOCs following chemical reactions are themselves generated by metabolic reactions triggered by microorganisms (figure 5).

To test discrimination, a radial basis function neural network was trained against approx 70% of the data set shown in figure 5 and tested against the remaining data to determine whether the microbial and chemical classes could be robustly discriminated. This gave a true positive rate of 0.88 and a true negative rate of 1.0 in discriminating these classes with a 94% average system accuracy due to the overlap between the two classes.

### *3.4. Kinetic parameters, sensitivity and limit of detection evaluation*

Reaction kinetic studies performed with this QCM-based biosensor prototype allowed calculation of theoretical affinity values based on the kinetics of the on/off response to a pulse of vapour. Figure 6 shows the modelled affinities to a range of compounds for the best and worst performing sensors; the *Hill*OBP_C57 sensor gave the highest affinity values towards isobutyraldehyde, 2-methylbutyraldehyde, isovaleraldehyde, butyric acid, while the lowest affinity values were observed from the *Hill*OBPs_C21691 sensor towards many compounds belonging to different chemical classes. On the other hand, all the *Hill*OBP-coated QCM exhibited a very slow frequency change in the detection of VOC vapours belonging to other chemical classes (terpenoids, ketones, esters, aromatics) (figure 6). These data are in agreement with the heat maps related to the OBPs gene expression level in *H. illucens* shown in Scieuzo *et al* [56], where the OBP_C57 was found to be the most expressed protein, with 100% identity between larvae and adults. Experimentally, another finding was obtained *in vitro*, through the binding assays in solution

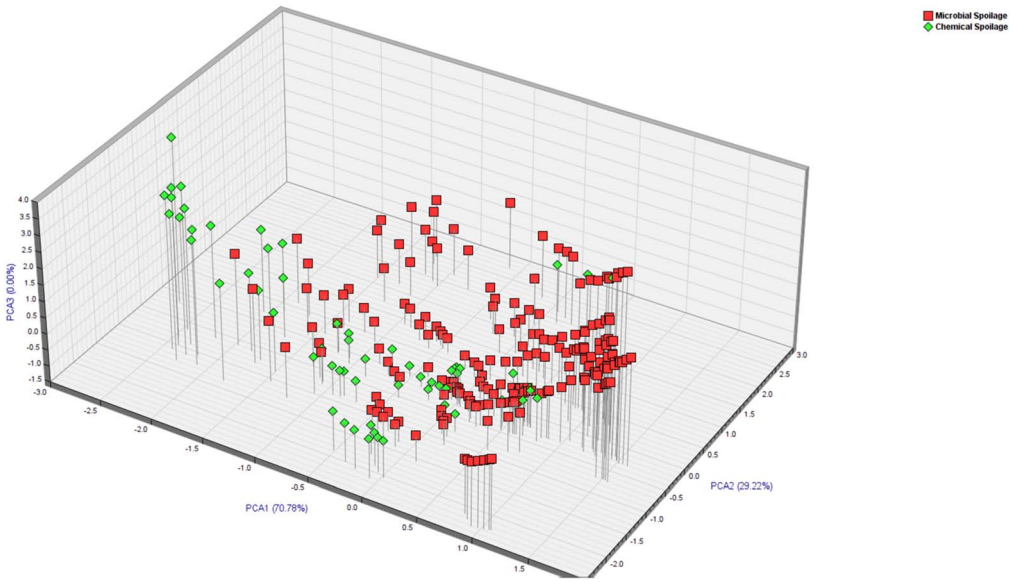


**Figure 5.** Principal Component Analysis (PCA) to discriminate VOCs of interest. The most significant differences between different VOCs, interacting with four *Hill*OBPs ($n = 9$ measurements for each VOC). VOCs were grouped in two classes, based on spoilage typology involved (microbial or chemical). The 3D plot depicts a spatial distribution map of *Hill*OBP-VOC interactions, underlining the biosensor ability to discriminate between these two different classes of VOCs.

(figure 3): *Hill*OBP_C57 showed the lowest levels of dissociation constants and, consequently, the highest levels of affinity in presence of the same VOC categories.

At the molecular level, biomolecular interactions were calculated starting from the equilibrium binding constant ($K_{eq}$) and the dynamic interactions between immobilized *Hill*OBPs and VOCs assuming the following equilibrium:

$$A + B \Leftrightarrow AB, \tag{2}$$

$$K_{eq} = \frac{[AB]}{[A][B]} = \frac{k_{on}}{k_{off}}, \tag{3}$$

where $[AB]$, $[A]$ and $[B]$ are equilibrium concentrations of the complex *Hill*OBP/VOC, free *Hill*OBP and free VOC respectively; $k_{on}$ and $k_{off}$ are time constants relative to the association/dissociation of the complex. The affinity and the strength of binding between *Hill*OBPs and VOCs were calculated as the ratio $k_{off}/k_{on}$ ($k = \Delta f$ / $\text{time}_{90\%}$), before the saturation was reached, as shown in figure 7. The sensor responses ($\Delta f$) were calculated as the differences between the corresponding *Hill*OBPs-coated QCM frequencies at the beginning and the end of the exposure phase of 4.0 ppm VOC vapour at room temperature. When the *Hill*OBPs were employed in the VOC ligand binding, the QCM response was a sudden decrease in frequency to the steady state level. The frequency returned to the original value, as a consequence of the fast and reversible binding between VOCs and *Hill*OBPs, within a time related to the binding affinity and difference in sensing responsivity was based on the different affinities of *Hill*OBPs with different chemical structures of VOCs belonging to the same chemical classes as shown in figure 6.

The changes in frequency of the QCMs were proportional to the concentration of VOCs to which they were exposed.

Isobutyraldehyde, 2-methylbutyraldehyde and isovaleraldehyde concentrations were initially set at 6.4 ppm and subsequently increased to 204.8 ppm, considering the saturation limit (table S5). As expected, the dynamic responses of *Hill*OBP_C57 sensor under exposure to increasing concentrations showed a good correlation with loading (frequency shifts) and a clear dependency between concentration and response. A Freundlich isotherm could be fitted to the concentration-response curves reflecting the adsorption/desorption of analytes on the QCMs (figure 8). Consequently, it was possible to calculate the *Hill*OBP_C57 sensor sensitivity (S, Hz $\text{ppm}^{-1}$) defined as the initial slope of the curves shown in figure 8. *Hill*OBP_C57 exhibited the highest sensitivity in presence of Isobutyraldehyde (5.45 Hz $\text{ppm}^{-1}$) with a correlation coefficient ($R^2$) of 0.98. Several reports indicated that the sensitivity of the QCM method depends largely on the molecular weight of the analyte [65, 66]. In this case, as 2-methylbutyraldehyde and isovaleraldehyde have the same molecular weight, the sensitivity is approximately equal. The correlation between frequency shift ($\Delta f$) plotted against VOC concentrations made it possible to determine, furthermore, the limit of detection (LOD) of the most interesting VOCs belonging to the aldehydes chemical class, for the *Hill*OBP_C57-coated sensor (table 1).

## 4. Discussion and conclusion

The molecular approaches allowed the heterologous production and purification in large amounts of recombinant OBPs from *Hermetia illucens* (*Hill*OBPs), using a bacterial expression system (*Escherichia coli*) and an engineered expression vector (pET-22b(+)) with or without His-tag. The best yields in terms of recombinant *Hill*OBPs production and the highest *in vitro* response, as well as the best single-molecule detection with biosensor device, were obtained with

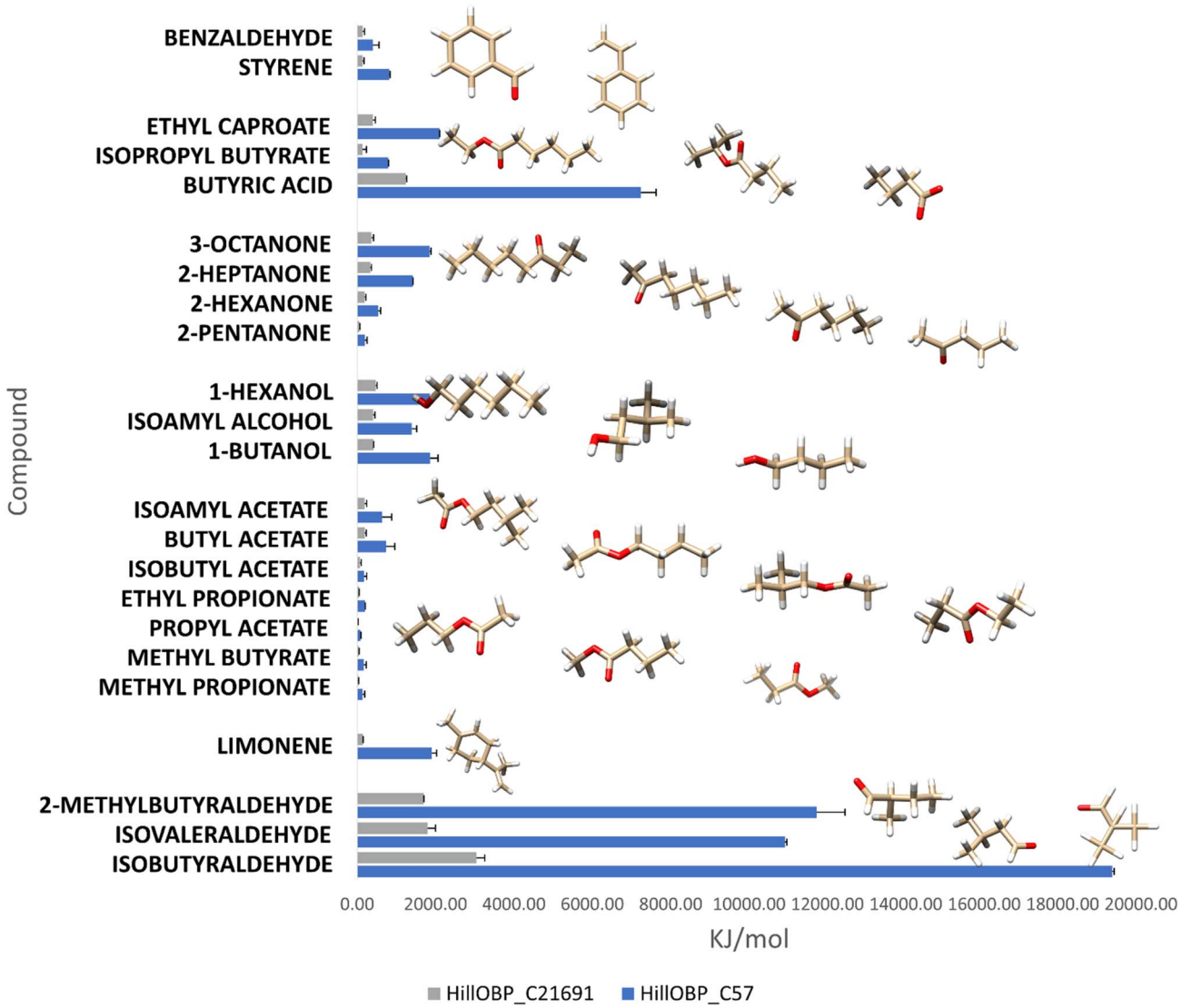


**Figure 6.** Comparison of affinities values (KJ $mol^{-1}$), following the QCM-based biosensor detection. The VOC structures most involved in food organic decomposition were analysed against models of the best and worst sensor, based on *Hill*OBP_C57 (blue) and *Hill*OBP_C21691 (grey), respectively. Among the most important VOCs involved in food organic degradation, the compounds belonging to the aldehyde chemical class exhibited the best levels of affinity, interacting with *Hill*OBP_C57. The data shown are from 9 replicate experiments.

the recombinant *Hill*OBP_C57 (His-tag free). The most plausible reason, supported by the molecular models *in silico* obtained [56], is the involvement of both N- and C-terminal in the main binding pocket, folded into a hydrophobic conformation; consequently, any tag could interfere with binding activities. Large amounts of encoded proteins from cloned cDNAs were possible thanks to some unique features of insect OBPs; they are small, water-soluble, extremely resistant to high temperatures and proteolytic degradation and able to refold even if treated in denaturing conditions. Moreover, using the *Hill*OBPs as biorecognition elements for VOCs of interest and QCMs as transducers, the well-known limits linked to fluorescent binding assays of micelles formation in solution were avoided. Although competitive binding assays confirmed the highest affinity towards the same VOCs previously screened during the biosensor test, the high value of the dissociation constant ($K_D \gg 1$ $\mu$M) measured with the 1-NPN probe to *HillOBPs* limited the accuracy of the competitive binding assays currently used. The results obtained with *in vitro* assays are reasonable, considering also the structural conformation of insect OBPs, that in absence of a gate-controlled entrance of ligands, reported instead for vertebrate OBPs, lead to a relatively high value of dissociation rates [67]. Results obtained with this innovative QCM-based biosensor capable of operating in the vapour phase are promising to overcome all the limits related to the *in vitro* evaluation of binding affinities with insect OBPs, providing an alternative method to the fluorescent binding assays [68, 69]. Artificial systems have recently been employed as biosensors for the detection of important ligands in complex environments, thus to some extent mimicking the olfactory system in detecting thousands of VOCs at very low concentrations (ppm or ppb). Indeed, biosensors with OBP recognition elements have been developed during recent years, but relatively few cases using insect OBPs have been reported, despite their unique thermal and chemical stability,

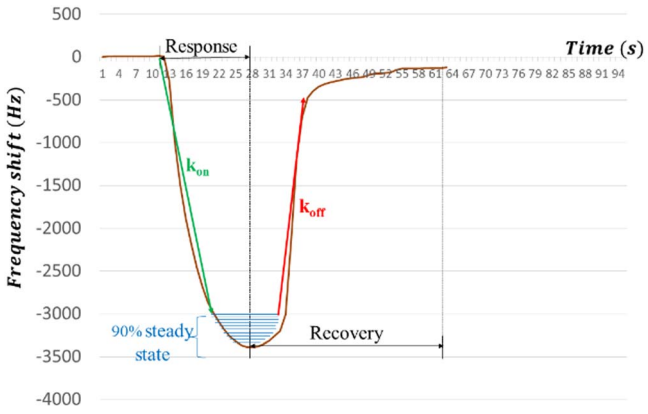


**Figure 7.** Response and recovery investigation of the *Hill*OBP_C57 sensor to isobutyraldehyde. A kinetic method for affinity calculations is based on time constants relative to the association/dissociation of protein-ligand complex. After exposure to the isobutyraldehyde vapour (4 ppm), the affinity value was calculated as a ratio between the dissociation (red arrow, $k_{off}$) and association (green arrow, $k_{on}$) constants, evaluated over a time equal to 90% of the total, to exclude the protein-ligand steady-state time (concave region of the curve). Recovery is considered optimal when, by injecting an adequate flow of fresh air, a stable baseline signal is restored.

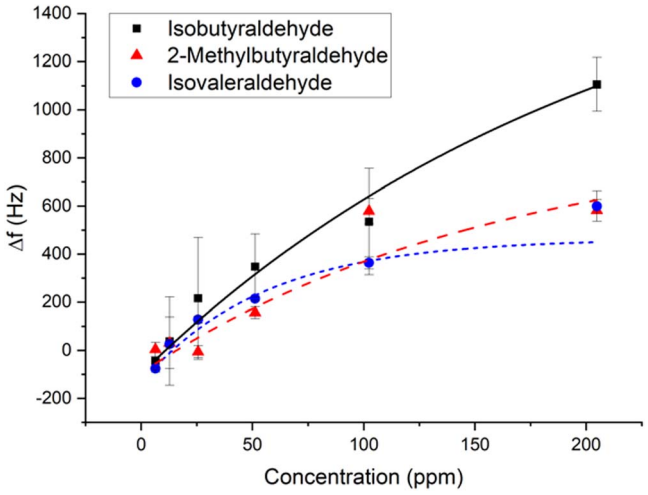


**Figure 8.** Frequency shifts of *Hill*OBP_C57 sensor in presence of VOCs, belonging to the same chemical class. Over a range of concentrations between 6.40 and 204.80 ppm, isobutyraldehyde, 2-methylbutyraldehyde and isovaleraldehyde a Freundlich isotherm could be fitted. Data are shown as the mean of three technical replicates, with error bars indicating the standard deviation.

which are important prerequisites for building robust, reliable and inexpensive devices [70–73]. From a pool of selected VOCs, emitted normally during organic decomposition processes, it was possible to identify specific ligands that interacted significantly with the analysed *Hill*OBPs. It emerged that only three immobilized *Hill*OBPs (*Hill*OBP_C57, *Hill*OBP_C11107 and *Hill*OBP_C1173), albeit with different affinities, were able to discriminate the VOC pool in the same way. The results showed that the *Hill*OBPs-based biosensor has a strong affinity for binding isobutyraldehyde, isovaleraldehyde, 2-methylbutyraldehyde and butyric acid at high and low concentrations in vapour phase. Isobutyraldehyde is characteristic for having a pungent odor, indicative of rancid fish [74]; isovaleraldehyde is predominant in oat grains, where the presence of molds is common [75] and in agreement with Scala *et al* [76], where the best bioconversion rates of *H. illucens* were recorded in presence of spent grain; butyric acid evokes a typical rancid smell, as the result of fermentation carried out by anaerobic bacteria, mainly belonging to the *Clostridium* genus [77]; 2-methylbutyraldehyde has been identified as one of the most important marker of lipid oxidation in food products [78] and for the selection of fresh and frozen/thawed fish [79]. High affinities between ligands and biosensor recognition layer can be also observed in the lower detection limits. The compounds identified in this study were considered the most specifically and selectively VOCs recognized by all the immobilized *Hill*OBPs; the QCM-based biosensor was able to detect their presence by changing the resonance frequencies, proportional to mass changes following the ligand binding, in a statistically significant way. In addition to these compounds, some other VOCs involved in microbial and chemical spoilage were also of considerable interest (table S4); the QCM-based biosensor detected their presence, but the intensity of resonance frequencies was not statistically significant. *Hill*OBPs interact without any great discrimination with many odorants but the binding affinity, i.e. the strength of interaction, was changed as shown by the different signal shapes. The quite analogous response of all the immobilised *Hill*OBPs on the QCM-based biosensor, towards the four identified VOCs, could be explained with the ecology of this insect. *H. illucens* is a species that during the larval stages grows in environments saturated with VOCs indicative of organic decomposition, so there is no need to develop extremely specific and selective OBPs [49; 80]. For this reason, *Hill*OBPs may have evolved in such a way that the specific binding for individual compounds is not necessary, but just receiving a bouquet of relevant compounds, this may contribute to the bioconverter insects' recognition and acceptance of a wide range of decomposing material. In conclusion, a QCM-biosensor prototype has been designed and optimized with *Hill*OBPs structures for biosensing applications, to make it possible the identification of interesting VOCs, that can be considered good markers of food organic degradation, in an extremely specific and selective way. The nanometre sized proteins allow a large number of binding sites to be available on a mass transducer, allowing biosensors to be constructed with high sensitivity to volatile compounds. The high performance of this prototype *Hill*OBP-based biosensor (high sensitivity, low limit of detection and good regeneration) may be of interest for further studies to allow the creation of a fast, inexpensive and reliable sensor for applications in the areas of environmental and agri-food monitoring.

**Table 1.** Calculated parameters based on the experimental responses of *Hill*OBP_C57 sensor. From each single analysis with a QCM-based biosensor, numerous parameters in terms of response time, affinity, sensitivity and limit of detection were evaluated. The limit of detection (LOD), defined as the minimum quantity that can be distinguished with more than 99% fidelity, was determined based on the ratio between the standard deviation ($\sigma$) and the sensor sensitivity ($S$) and it was calculated as $3.3 \times \sigma/S$.

| Compound | CAS No. | Response time (s) | Affinity ($\mu M^{-1}$) | Sensitivity (Hz $ppm^{-}$) | $R^2$ Coefficient | Limit of detection (ppm) |
|---|---|---|---|---|---|---|
| Isobutyraldehyde | 78-84-2 | 7 | 1.91 | 5.45 | 0.98 | 0.013 |
| Isovaleraldehyde | 590-86-3 | 11 | 1.66 | 3.12 | 0.94 | 0.004 |
| 2-Methylbutyraldehyde | 96-17-3 | 25 | 0.64 | 3.34 | 0.81 | 0.024 |

## Acknowledgments

This work was supported by *Programma Operativo Nazionale Ricerca e Innovazione 2014 -2020* (CCI 2014IT16M2OP005) within the framework of *Fondo Sociale Europeo, Azione I.1* 'Dottorati Innovativi con caratterizzazione industriale' and by Basilicata Region within the framework of 'Programma di Sviluppo Rurale 2014–2020' (project 'FeedInsect'—measure 16.2, D.D. 424 of 21/05/2019).

## Data availability statement

All data that support the findings of this study are included within the article (and any supplementary files).

## ORCID iDs

Marisa Nardiello https://orcid.org/0000-0002-3506-5029
Krishna C Persaud https://orcid.org/0000-0001-5730-9568

## References

[1] Schiffman S S, Gutierrez-Osuna R and Nagle H T 2001 Use of an electronic nose to evaluate odors from swine operations *Artificial Chemical Sensing: Olfaction and the Electronic Nose* (*Electrochemical Society Proceedings* 2001) 15 (New Jersey: The Electrochemical Society Inc) pp 200–5 ISOEN (2001) Washington DC

[2] Ruth J H 1986 Odor thresholds and irritation levels of several chemical substances: a review *Am. Ind. Hyg. Assoc. J.* **47** A-142

[3] Conti C, Guarino M and Bacenetti J 2020 Measurements techniques and models to assess odor annoyance: a review *Environ. Int.* **134** 105261

[4] Hernández-Mesa M, Ropartz D, García-Campaña A M, Rogniaux H, Dervilly-Pinel G and Le Bizec B 2019 Ion mobility spectrometry in food analysis: principles, current applications and future trends *Molecules* **24** 2706

[5] Flores E, Viallon J, Moussay P and Wielgosz R I 2013 Accurate Fourier transform infrared (FT-IR) spectroscopy measurements of nitrogen dioxide ($NO_2$) and nitric acid ($HNO_3$) calibrated with synthetic spectra *Appl. Spectrosc.* **67** 1171–8

[6] Biasioli F, Gasperi F, Yeretzian C and Märk T D 2011 PTR-MS monitoring of VOCs and BVOCs in food science and technology *Trends Analyt. Chem.* **30** 968–77

[7] Bennett J W and Inamdar A A 2015 Are some fungal volatile organic compounds (VOCs) mycotoxins? *Toxins* **7** 3785–804

[8] Srivastava A K, Dev A and Karmakar S 2018 Nanosensors and nanobiosensors in food and agriculture *Environ. Chem. Lett.* **16** 161–82

[9] Zanardi E, Caligiani A and Novelli E 2018 New insights to detect irradiated food: an overview *Food Anal. Methods* **11** 224–35

[10] Boumnijel I, Ben Amor H, Chekir H and Hajji N 2016 Hydrogen sulphide removal from the effluents of a phosphoric acid production unit by absorption into chlorinated seawater under alkaline conditions *C. R. Chim.* **19** 517–24

[11] Lewkowska P, Cieślik B, Dymerski T, Konieczka P and Namieśnik J 2016 Characteristics of odors emitted from municipal waste water treatment plant and methods for their identification and deodorization techniques *Environ. Res.* **151** 573–86

[12] Zhou Y, Hallis S A, Vitko T and Suffet I H 2016 Identification, quantification and treatment of fecal odors released into the air at two wastewater treatment plants *J. Environ. Manag.* **180** 257–63

[13] Lucernoni F, Tapparo F, Capelli L and Sironi S 2016 Evaluation of an odour emission factor (OEF) to estimate odour emissions from landfill surfaces *Atmos. Environ.* **144** 87–99

[14] Van der Heyden C, Demeyer P and Volcke E I P 2015 Mitigating emissions from pig and poultry housing facilities through air scrubbers and biofilters: state-of-the-art and perspectives *Biosyst. Eng.* **134** 74–93

[15] Wang X, Xie B, Wu D, Hassan M and Huang C 2015 Characteristics and risks of secondary pollutants generation during compression and transfer of municipal solid waste in Shanghai *Waste Manag.* **43** 1–8

[16] Covington J A, Marco S, Persaud K C, Schiffman S S and Nagle H T 2021 Artificial Olfaction in the 21st Century *IEEE Sens. J.* **21** 12969–90

[17] Stuetz R M M, Fenner R A A and Engin G 1999 Characterisation of wastewater using an electronic nose *Water Res.* **33** 442–52

[18] Tanaka M, Anguri H, Nonaka A, Kataoka K, Nagata H, Kita J and Shizukuishi S 2004 Clinical assessment of oral malodor by the electronic nose system *J. Dent. Res.* **83** 317–21

[19] Wilson A D 2012 Review of electronic-nose technologies and algorithms to detect hazardous chemicals in the environment *Proc. Technol.* **1** 453–63

[20] Schnürer J, Olsson J and Börjesson T 1999 Fungal volatiles as indicators of food and feeds spoilage *Fungal Genet. Biol.* **27** 209–17

[21] Lee H D and Lim H J 2012 Real-time monitoring systems for malodor compounds sources using ubiquitous sensor networks *J. Korea Acad.-Ind. Cooperation Soc.* **13** 856–65

[22] Persaud K C 2012 Biomimetic olfactory sensors *IEEE Sens. J.* **12** 3108–12

[23] Pelosi P, Baldaccini N E and Pisanelli A M 1982 Identification of a specific olfactory receptor for 2-isobutyl-3-methoxypyrazine *Biochem. J* **201** 245–8

[24] Vogt R G and Riddiford L M 1981 Pheromone binding and inactivation by moth antennae *Nature* **293** 161–3

[25] Flower D R 1996 The lipocalin protein family: structure and function *Biochem. J* **318** 1–14

[26] Flower D R, North A C T and Sansom C E 2000 The lipocalin protein family: structural and sequence overview *Biochim. Biophys. Acta* **1482** 9–24

[27] Pelosi P 1998 Odorant-binding proteins: structural aspects *Ann. N.Y. Acad. Sci.* **855** 281–93

[28] Leite N R, Krogh R, Xu W, Ishida Y, Iulek J, Leal W S and Oliva G 2009 Structure of an odorant-binding protein from the mosquito Aedes aegypti suggests a binding pocket covered by a pH-sensitive 'Lid' *PLoS One* **4** e8006

[29] Pelosi P, Iovinella I, Felicioli A and Dani F R 2014 Soluble proteins of chemical communication: an overview across arthropods *Front. Physiol.* **5** 320

[30] Honson N S, Gong Y and Plettner E 2005 Structure and function of insect odorant and pheromone-binding proteins (OBPs and PBPs) and chemosensory-specific proteins (CSPs) *Recent Adv. Phytochem.* (*Chemical Ecology and Phytochemistry of Forest Ecosystems* 39) ed J T Romeo (The Netherlands: Elsevier) 9 227–68

[31] Böcskei Z, Groom C R, Flower D R, Wright C E, Phillips S E, Cavaggioni A, Findlay J B C and North A C T 1992 Pheromone binding to two rodent urinary proteins revealed by x-ray crystallography *Nature* **360** 186–8

[32] Cavaggioni A, Mucignat C and Tirindelli R 1999 Pheromone signalling in the mouse: role of urinary proteins and vomeronasal organ *Arch. Ital. Biol.* **137** 193–200 PMID: 10349497

[33] Marchese S, Pes D, Scaloni A, Carbone V and Pelosi P 1998 Lipocalins of boar salivary glands binding odours and pheromones *Eur. J. Biochem.* **252** 563–8

[34] Scaloni A, Monti M, Angeli S and Pelosi P 1999 Structural analysis and disulfide-bridge pairing of two odorant-binding proteins from *Bombyx mori Biochem. Biophys. Res. Commun.* **266** 386- 391

[35] Pelosi P, Zhu J and Knoll W 2018 From radioactive ligands to biosensors: binding methods with olfactory proteins *Appl. Microbiol. Biotechnol.* **102** 8213–27

[36] Ricatti J *et al* 2019 Effects of point mutations in the binding pocket of the mouse major urinary protein MUP20 on ligand affinity and specificity *Sci. Rep.* **9** 1–12

[37] Persaud K C and Tuccori E 2014 Biosensors Based on Odorant Binding Proteins *Bioelectronic Nose* (Netherlands: Springer) 171–90

[38] Persaud K and Tuccori E 2020 Biosensors using odorant binding proteins from bombyx mori *Chem. Sens.* **45** 148

[39] Sankaran S, Panigrahi S, Sanku and Mallik S 2011 Odorant binding protein based biomimetic sensors for detection of alcohols associated with Salmonella contamination in packaged beef *Biosens. Bioelectron.* **26** 3103–9

[40] Di Pietrantonio F, Cannatà D, Benetti M, Verona E, Varriale A, Staiano M and D'Auria S 2013 Detection of odorant molecules via surface acoustic wave biosensor array based on odorant-binding proteins *Biosens. Bioelectron.* **41** 328–34

[41] Tuccori E and Persaud K C 2019 Pheromone detection using odorant binding protein sensors *IEEE International Symposium on Olfaction and Electronic Nose (ISOEN) (2019pp 1–3*

[42] Cali K and Persaud K C 2020 Modification of an *Anopheles gambiae* odorant binding protein to create an array of chemical sensors for detection of drugs *Sci. Rep.* **10** 3890

[43] Franco A, Scieuzo C, Salvia R, Petrone A M, Tafi E, Moretta A, Schmitt E and Falabella P 2021 Lipids from *Hermetia illucens*, an innovative and sustainable source *Sustainability* **13** 10198

[44] Hahn T, Tafi E, Aman P, Salvia R, Falabella P and Zibek S 2020 Current state of chitin purification and chitosan production from insects *J. Chem. Technol. Biotechnol.* **95** 2775–95

[45] Triunfo M, Tafi E, Guarnieri A, Scieuzo C, Hahn T, Zibek S, Salvia R and Falabella P 2021 Insect chitin-based nanomaterials for innovative cosmetics and cosmeceuticals *Cosmetics* **8** 40

[46] Moretta A, Salvia R, Scieuzo C, Di Somma A, Vogel H, Pucci P, Sgambato A, Wolff M and Falabella P 2020 A bioinformatic study of antimicrobial peptides identified in the black soldier Fly (BSF) *Hermetia illucens* (diptera: stratiomyidae) *Sci. Rep.* **10** 16875

[47] Manniello M D, Moretta A, Salvia R, Scieuzo C, Lucchetti D, Vogel H, Sgambato A and Falabella P 2021 Insect antimicrobial peptides: Potential weapons to counteract the antibiotic resistance *Cell. Mol. Life Sci.* **1** 3

[48] Moretta A *et al* 2021 Antimicrobial peptides: a new hope in biomedical and pharmaceutical fields *Front. Cell Infect. Microbiol.* **11** 453

[49] Zheng L *et al* 2013 Bacteria mediate oviposition by the black soldier fly, *Hermetia illucens* (L.), (diptera: stratiomyidae) *Sci. Rep.* **3** 2563

[50] Jucker C, Erba D, Leonardi M G, Lupi D and Savoldelli S 2017 Assessment of vegetable and fruit substrates as potential rearing media for *Hermetia illucens* (Diptera: Stratiomyidae) larvae *Environ. Entomol.* **46** 1415–23

[51] Charlton A J *et al* 2015 Exploring the chemical safety of fly larvae as a source of protein for animal feed *J. Insects Food Feed* **1** 7–16

[52] Alvarez L 2012 The role of black soldier fly, Hermetia illucens (L.) (diptera: stratiomyidae) in sustainable waste management in northern climates PhD Thesis University of Windsor, Canada Electronic Theses and Dissertations. 402. (https://scholar.uwindsor.ca/etd/402)

[53] Wang Y S and Shelomi M 2017 Review of black soldier fly (*Hermetia illucens*) as animal feed and human food *Foods* **6** 91

[54] Pezzi M *et al* 2021 Fine structure of maxillary palps in adults of *Hermetia illucens* (diptera: stratiomyidae) *J. Med. Entomol.* **58** 658–65

[55] Kim W, Bae S, Lee S, Choi Y, Han S and Koh Y H 2011 Biochemical characterization of digestive enzymes in the black soldier fly, Hermetia illucens (diptera: Stratiomyidae) *J. Asia Pac. Entomol.* **14** 11–4

[56] Scieuzo C *et al* 2021 *Hermetia illucens* (L.) (diptera: stratiomyidae) odorant binding proteins and their interactions with selected volatile organic compounds: an in silico approach *Insects* **12** 814

[57] Lowry O H, Rosenbrough N J, Farr A L and Randall R J 1951 Protein measurement with the folin phenol reagent *J. Biol. Chem.* **193** 265–75

[58] Swinehart D F 1962 The beer–lambert law *J. Chem. Educ.* **39** 333

[59] Sauerbrey G Z 1959 The use of quarts oscillators for weighing thin layers and for microweighing *Z. Phys.* **155** 206–22

[60] Pearson K 1901 On lines and planes of closest fit to systems of points in space *Philos. Mag.* **2** 559–72

[61] Hotelling H 1933 Analysis of a complex of statistical variables into principal components *J. Educ. Psychol.* **24** 417–41

[62] Hotelling H 1936 Relations between two sets of variates *Biometrika* **28** 321–77

[63] Sun Y S, Luo J, Lam K S and Zhu X D 2013 Detection of formation and disintegration of micelles by oblique-incidence

reflectivity difference microscopy *Instrum. Sci. Technol.* **41** 545–55
[64] Knoll W, Hara M and Tamada K 1998 Suprabiomolecular architectures at functionalized surfaces *Micelles, Microemulsions, and Monolayers* (Boca Raton: Routledge)
[65] Triyana K, Sembiring A, Rianjanu A, Hidayat S N, Riowirawan R, Julian T, Kusumaatmaja A, Santoso I and Roto R 2018 Chitosan-based quartz crystal microbalance for alcohol sensing *Electronics* **7** 181
[66] Ayad M M, El-Hefnawey G and Torad N L 2009 A sensor of alcohol vapours based on thin polyaniline base film and quartz crystal microbalance *J. Hazard. Mater.* **168** 85–8
[67] Pelosi P, Mastrogiacomo R, Iovinella I, Tuccori E and Persaud K C 2014 Structure and biotechnological applications of odorant-binding proteins *Appl. Microbiol. Biotechnol.* **98** 61–70
[68] Pelosi P, Zhu J and Knoll W 2018 Odorant-binding proteins as sensing elements for odour monitoring *Sensors* **18** 3248
[69] Tan J, Zaremska V, Lim S, Knoll W and Pelosi P 2020 Probe-dependence of competitive fluorescent ligand binding assays to odorant-binding proteins *Anal. Bioanal. Chem.* **412** 547–54
[70] Vogt R G, Prestwich G D and Lerner M R 1991 Odorant-binding-protein subfamilies associate with distinct classes of olfactory receptor neurons in insects *J. Neurobiol.* **22** 74–84
[71] Dal Monte M, Centini M, Anselmi C and Pelosi P 1993 Binding of selected odorants to bovine and porcine odorant-binding proteins *Chem. Sens.* **18** 713–21
[72] Hou Y *et al* 2005 Study of langmuir and langmuir−blodgett films of odorant-binding protein/amphiphile for odorant biosensors *Langmuir* **21** 4058–65
[73] Wei Y, Brandazza A and Pelosi P 2008 Binding of polycyclic aromatic hydrocarbons to mutants of odorant-binding protein: a first step towards biosensors for environmental monitoring *BBA—Proteins Proteom.* **1784** 666–71
[74] Fukami K, Ishiyama S, Yaguramaki H, Masuzawa T, Nabeta Y, Endo K and Shimoda M 2002 Identification of distinctive volatile compounds in fish sauce *J. Agric. Food Chem.* **50** 5412–6
[75] Lippolis V, Pascale M, Cervellieri S, Damascelli A and Visconti A 2014 Screening of deoxynivalenol contamination in durum wheat by MOS-based electronic nose and identification of the relevant pattern of volatile compounds *Food Control* **37** 263–71
[76] Scala A, Cammack J A, Salvia R, Scieuzo C, Franco A, Bufo S A, Tomberlin J K and Falabella P 2020 Rearing substrate impacts growth and macronutrient composition of *Hermetia illucens* (L.) (diptera: stratiomyidae) larvae produced at an industrial scale *Sci. Rep.* **10** 19448
[77] Ciani M, Comitini F, Mannazzu I and Domizio P 2010 Controlled mixed culture fermentation: a new perspective on the use of non-Saccharomyces yeasts in winemaking *FEMS Yeast Res.* **10** 123–33
[78] Lee B H 2014 *Fundamentals of food biotechnology* (China: Wiley)
[79] Leduc F, Krzewinski F, Le Fur B, N'Guessan A, Malle P, Kol O and Duflos G 2012 Differentiation of fresh and frozen/thawed fish, European sea bass (*Dicentrarchus labrax*), gilthead seabream (*Sparus aurata*), cod (*Gadus morhua*) and salmon (*Salmo salar*), using volatile compounds by SPME/GC/MS *J. Sci. Food Agric.* **92** 2560–8
[80] Hoc B, Noël G, Carpentier J, Francis F, Caparros and Megido R 2019 Optimization of black soldier fly (*Hermetia illucens*) artificial reproduction *PLoS One* **14** 0216160